This is a previous version of the article published by Wiley-VCH Verlag GmbH & Co. KGaA in ChemElectroChem. 2015, 2(7): 958-962. doi:10.1002/celc.201500084

Electrochemical oxidation of small organic molecules on Au nanoparticles with preferential surface orientation

J. Monzó[a], Y. Malewski[a], F. J. Vidal-Iglesias[b], J. Solla-Gullón[b] and P. Rodriguez[a]

[a] University of Birmingham. School of Chemistry, Birmingham. B15 2TT, UK.

[b] Institute of Electrochemistry, University of Alicante, E-03080, Alicante, Spain.

Corresponding author: p.b.rodriguez@bham.ac.uk

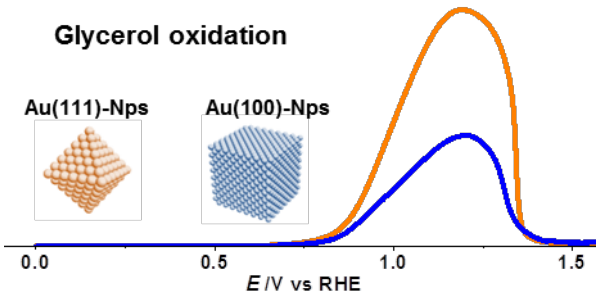

Keywords: Gold, nanoparticles, preferential surface orientation, alcohol oxidation.

Abstract

The surface orientation effect on the oxidation of small organic molecules such as methanol, formaldehyde, ethanol and glycerol has been studied on Au nanoparticles in alkaline medium. Two sets of Au nanoparticles enriched in (100) and (111) facets were synthetized by using colloidal methods in presence of cetyltrimethylammonium bromide (CTAB). The nanoparticles were physically characterized by TEM and XRD and electrochemically characterized by using Pb UPD as surface structure probe. It is reported that while methanol oxidation was similar in both types of nanoparticles, the oxidation of formaldehyde presented a clear surface orientation effect. For this reaction, the nanoparticles with (111) preferential orientation presented higher

current densities at low potentials, whereas Au(100) nanoparticles exhibited higher activity at more positive potentials than 1.0 V vs RHE. On the other hand, for glycerol and ethanol oxidations, the onset of the reaction was similar in both types of particles, although Au(111) nanoparticles showed higher current densities than the Au(100) ones.

1. Introduction

During the last decades, the search for materials with enhanced catalytic activity toward the oxidation of potential alcohols and their intermediates to be used in power sources has increased exponentially[1-4]. Besides the search of new alloy materials, special attention has been paid to the effect of the composition of the electrolyte[5-11]. In acidic media, among all the metals, Pt and Pd are the metal catalysts of choice for the oxidation of many organic molecules. Inclusive, the search for suitable alloys with higher catalytic activity is mainly based on Pt alloys including in the matrix metals as Bi[12-15], Pb[16,17], Sn[18,19] or Mo[20,21] among others.

On the other hand, in alkaline media, Au electrodes are quite often more active than Pt and Pd electrodes towards the oxidation of carbon monoxide and some small organic molecules[5-8,22-24]. Interestingly, this is not always the case since for glycerol, the catalytic activity of Pt/C and Pd/C is superior to the activity of Au/C.[25,26] The main reason for the high catalytic activity of gold is the lower propensity of gold to form surface oxides, which inhibit the alcohol oxidation activity[27-29]. Therefore, the high catalytic activity of gold for the electrochemical oxidation of alcohols in alkaline media has little to do with special catalytic properties of gold, but rather with the favourable reaction conditions in solution (i.e. effect of the pH in decoupled proton–electron transfer steps)[7] combined with the low tendency of gold to become poisoned by either CO or surface oxides (i.e. weak adsorption properties of intermediates).

In addition to the effect of the pH, only few works have included the influence of the surface structure on the catalytic activity of gold [24]. In particular the role of the surface structure of gold towards the oxidation of methanol, ethanol and glycerol has been under looked and scarce contributions can be found in the literature[22,27-33]. Additionally, even fewer contributions have been published dealing with the alcohol oxidation on nanoparticulated systems[34-37]. Consequently, the aim of this work is to explore the electrocatalytic properties of two shape-controlled Au nanoparticles towards the oxidation of formaldehyde and some alcohols, including methanol, ethanol and glycerol, in alkaline solution.

2. Experimental section

2.1 Synthesis of Au nanoparticles

Cubic nanoparticles were synthetized by a colloidal seed-mediated method, using spherical gold nanoparticles as seeds, following the experimental procedure described by Murphy and Sau[38]. Briefly, Au seeds were prepared by the reduction of $HAuCl_4 \cdot 3H_2O$ (2.5×10^{-4} M) by ice-cold $NaBH_4$ (6.0×10^{-4} M) in the presence of CTAB (7.5×10^{-2} M). Au seeds were used to induce the nanocubes formation in a growth solution containing $HAuCl_4$ (2×10^{-4} M) + CTAB (1.6×10^{-2} M) + L-ascorbic acid (6×10^{-2} M) to which Au seeds (1.25×10^{-8} M) were added.

On the other hand, the octahedral/tetrahedral nanoparticles were synthesized using a similar methodology to that previously described by Han et al.[39,40]. In brief, an aqueous solution of L-ascorbic acid (5×10^{-4} M) was added to a growth solution containing $HAuCl_4$ (1.25×10^{-4} M) and CTAB (10 mM). Then, Au particle formation was induced by adding NaOH (100 mM).

In both cases, after the reaction was completed, the solution was centrifuged at 3000 rpm for 30 minutes to precipitate the solid and remove the excess of reactants. Then, Au nanoparticles were redispersed in ultra-pure water, and their precipitation was induced with the addition of NaOH which destabilized the CTAB adsorbed on the surface of the Au nanoparticles producing nanoparticle precipitation. The nanoparticles were again collected by centrifugation and the supernatant discarded. Then, the Au nanoparticles were cleaned 2-3 times with ultra-pure water following the same process of centrifugation and redispersion in ultra-pure water. This protocol allows the removal of as much CTAB from the surface of the particles as possible.

2.2 Characterization of the nanoparticles

Transmission Electron Microscopy (TEM) was performed using a JEOL JEM 1200 EX MKI instrument. Samples were prepared by drop-casting ethanolic suspensions of each catalyst on carbon-coated copper grids and drying in air.

X-ray diffraction (XRD) patterns were obtained with a Bruker AXS D2 PHASER diffractometer using CoKα (0.179 nm) radiation. Samples were prepared by depositing a couple of drops (20 µL) of the CTAB protected nanoparticles on a quartz holder and drying in air.

2.3 Electrochemical measurements

In order to obtain very clean and reproducible conditions, prior to each experimental session, the cell and all glassware were immersed overnight in an acidic solution of $KMnO_4$. Next the solution was removed and the residual MnO_4^- was rinsed with an acidic solution of H_2O_2 and sulphuric acid (3:1) and finally thoroughly washed several times by boiling with ultra-pure water (Elga PureUltra, 18.2 MΩ cm, 1 ppb total organic carbon). A two-compartment electrochemical cell was employed, with a gold

wire as counter electrode and a reversible hydrogen electrode (RHE) as the reference electrode. Electrochemical measurements were performed with an Autolab PGSTAT12. Solutions were prepared from NaOH (99.99 %, Sigma-Aldrich), and ultra-pure water. Argon (Ar, (N66)) was used to deoxygenate all solutions. Au nanoparticles were deposited on a glassy carbon rod (SIGRADUR) electrode with 2.0 mm diameter which was polished before each experiment with diamond alumina.

3. Results and discussion

3.1 Characterization of the preferential oriented nanoparticles

Figures 1A-B show the transmission electron microscopy (TEM) images and the corresponding X-ray diffraction (XRD) patterns of the two different samples of gold nanoparticles employed in this work. The TEM images indicate the presence of Au cubes and octahedrons with a particle size of about 45-50 nm in agreement with a previous contribution[41]. Thus, whereas the cubic nanoparticles (fig.1A) suggest the presence of (100) facets, the octahedral/tetrahedral ones (fig.1B) should have a preferential (111) surface orientation. This fact is confirmed by the XRD patterns shown in figure 1A-B respectively. The XRD patterns of the different Au nanoparticles clearly show a distinct relative intensity of the different diffraction peaks indicating the presence of a preferential orientation parallel to the substrate in agreement with previous observations by M. Eguchi, et al.[42]

In addition to the TEM and XRD analyses, the electrochemical characterization of the nanoparticles was performed by using Pb underpotential deposition (UPD) in order to proof the existence of the preferential surface sites and the absence of undesirable faceting[43,44]. The Pb UPD on gold single-crystal electrodes has shown surface structure dependence and has been used for the characterization of preferential

oriented nanoparticles[45]. Figure 2A shows the Pb UPD on both types of gold nanoparticles. In the positive cycle (Pb dissolution) 4 main contributions can be distinguished. The voltammetric signal at ca. 0.44 V (RHE) has been associated with the dissolution of Pb adsorbed on the (111) terrace sites, while the signals at ca. 0.38 and 0.47 V (RHE) have been ascribed to the presence of (100) terraces. Finally, the contribution at 0.56 V (RHE) corresponds to the presence of (110) and defect surface sites. As can be seen, the results found here are in good agreement with the results obtained from ex situ TEM and XRD experiments and reveal a high contribution of (100) and (111) surface sites on the cubic and octahedral/tetrahedral nanoparticles, respectively.

In addition to the surface characterization using the Pb UPD, the formation of PbO_2 layers at potentials higher than 1.1 V vs RHE also promote the oxidation of organic contaminants from the electrode[43,44]. Subsequently, in order to remove the Pb/PbO_2 after the electrochemical cleaning process, the supported particles were dipped in 0.1 M HNO_3 for 10 minutes[46]. Figure 2B shows the blank voltammetric response of the Au nanoparticles after this cleaning procedure. As can be seen in the voltammetry, no peaks were observed between 0.25 and 0.8 V, which confirms the absence of residual Pb from the cleaning procedure. The peaks at 1.2 V vs RHE in the positive scan and at 1.1 V in the negative scan correspond to the formation and reduction of gold oxides respectively. In particular, the peak at 1.28 V is attributed to the oxide formation on (111) sites while the peak at 1.40 V is characteristic of the oxide formation on (100) sites.[47]

In order to properly normalize the catalytic activity, the electrochemical active surface area of the nanoparticles was calculated both by using the charges of the Pb UPD[40,41] and the Au oxide reduction [48,49] .The electrochemical surface area of Au

electrode was determined from the reduction of the monolayer of gold oxide. The charge of the reduction of monolayer gold oxide on a polyoriented electrode, when the anodic limit of the voltammogram is set just before the onset of oxygen evolution reaction, is 420 μCcm^{-2} [49]. On the other hand, for the upd process between 0.25 and 0.70 V a charge density value of 420 $\mu C\ cm^{-2}$ was used to determine the surface area of the nanoparticles. Table 1 summarizes the values of the electrochemical active surface areas determined by both methods.

Table 1. Electrochemical surface area (cm^2) of cubic and octahedral/tetrahedral nanoparticles determined by Pb UPD and Au oxide reduction.

Sample/Method	Pb UPD	Au oxide reduction
Cubic	**0.0333 cm^2**	**0.0359 cm^2**
Octa/tetrahedral	**0.0325 cm^2**	**0.0349 cm^2**

3.2 Electrochemical oxidation of carbon monoxide, methanol and formaldehyde

It has been previously shown that gold catalyses the methanol oxidation in alkaline media at low potentials on very rough surfaces[9]. Intuitively, this effect could be attributed to the high catalytic activity of low coordinated atoms on the surface of the electrode. Based on spectroscopic observations, it has been proposed that during methanol oxidation the first step is always the dehydrogenation of the methyl group followed by the formation of formaldehyde, formic acid and CO as stable intermediates[50,51]. Therefore, the oxidation of methanol and its oxidation reaction intermediates on the preferential oriented nanoparticles is of high interest in order to elucidate the reaction mechanism on these types of catalysts. Previous studies have also shown that the adsorption of one CO monolayer on a gold electrode in alkaline

media takes places at lower potentials than 0.3 V vs RHE with further oxidation at potentials higher than 0.7 V[30-32]. Inclusive, additional studies have shown that the CO adsorbed on Au(111) and Au(100) promotes the oxidation of methanol and other alcohols[52]. In order to evaluate the surface selectivity of CO oxidation on the Au preferentially oriented nanoparticles, a similar procedure than that used in ref [32] was followed. In brief, the electrolyte was saturated with carbon monoxide after bubbling through the solution for 3 min under potential control and subsequently purging with Ar for 30 min so as to remove all CO from solution. The resulting cyclic voltammetries have shown no difference with respect to the blank voltammetries, which suggests the poor interaction of CO on Au nanoparticles even upon adsorption at low potentials, regardless of their shape/preferential surface structure. The differences between the single-crystal behaviour and the nanoparticles might be attributed to the lack of long order surface structure on the facets of the nanoparticles[53,54] or to the higher surface energy of the nanoparticles. It has been shown that the oxidation of irreversibly adsorbed CO is strongly dependent on the presence of long order (111) sites on the surface[32]. The bulk oxidation of carbon monoxide on the nanoparticles did not show surface structure sensitivity in agreement to those results described previously in the literature [22,31,55].

Figures 3A-B show the voltammetric profiles of methanol and formaldehyde on the cubic and octahedral Au nanoparticles in alkaline medium. For methanol, as can be seen in figure 3A, the voltammetric profiles are quite similar both in terms of the onset of the oxidation (ca. 0.6 V) and recorded current densities. Even though the differences are subtle, it is important to note that the octahedral nanoparticles present slightly higher current densities between 0.75 and 0.9 V, while at higher potentials, the cubic nanoparticles present a higher catalytic activity. It is widely-

accepted that the most important reactive intermediate species on the oxidation of methanol is formaldehyde [29]. In this regard, figure 3B reports the voltammetric responses obtained on both Au nanoparticles towards the direct oxidation of this intermediate (formaldehyde). Clear similarities can be found between methanol and formaldehyde electrochemical oxidations. In particular, and despite the formaldehyde oxidation occurs at much lower potentials than the methanol oxidation (ca. 0.3 V vs RHE), in both cases the current densities obtained on the (111) preferentially oriented nanoparticles are higher at low potentials (up to 0.95 V) while the Au cubic nanoparticles are more active at potentials higher than 1.0 V. Previous FTIR measurements have indicated that formate is the final product of the oxidation of formaldehyde when the potential is limited to 1.5 V and cannot be further oxidized[29,31,55,56].

3.3 Electrochemical oxidation of ethanol and glycerol

Since the adsorption and oxidation of small organic molecules have shown surface structure sensitivity[22,24-30], it is expected that the adsorption of C2 and C3 molecules might be also affected by the surface orientation of the electrocatalyst.

The role of the surface structure in the electrochemical oxidation of ethanol in alkaline medium, has not been extensively studied[28]. Very recently, it has been shown that the presence of defects on the surface of the electrode promotes the oxidation of ethanol at low overpotentials, although at higher potentials (ca. 1 V), Au(111) has shown the highest catalytic activity in comparison with Au(100) and Au(110) electrodes[33]. This can be associated to the adsorption strength of OH and the gold oxide formation. Interestingly, it has been also shown that the only product of ethanol oxidation on gold electrodes in alkaline media is acetate, regardless of the electrode's orientation[28].

Figure 4A shows the voltammetric profiles of the cubic and octahedral Au nanoparticles towards the oxidation of ethanol in alkaline medium. As can be seen, both types of nanoparticles show a similar voltammetric profile and a similar onset oxidation potential. However, the Au nanoparticles with (111) preferential orientation displayed higher current densities during the whole potential range. Even though the Au nanoparticles are preferentially oriented, the appearance of a pre-peak at 0.75 V is an indication of the presence of defects on the surface as expected from nanoparticulated materials.

The electrochemical oxidation of glycerol is a reaction that has recently been studied extensively on gold electrodes. However, to our knowledge, there is just one work available regarding the oxidation of glycerol on Au(100) electrode[28]. Figure 4B shows the electrochemical oxidation of glycerol in alkaline medium on the cubic and octahedral Au nanoparticles. As can be seen, once again the nanoparticles with (111) preferential orientation show a higher catalytic activity. In addition, the current density values for the oxidation of glycerol on the cubic nanoparticles are in agreement with the value reported by Avramov-Ivic et al. for the Au(100) single crystal electrode[28]. Concerning the reaction products, it is known that, in alkaline media, the main oxidation products for glycerol oxidation are glycolate and formate[6]. Moreover, Fernandes Gomes et al. also reported the formation of dihydroxyacetone, tartronic acid, mesoxalic acid, glyoxylic acid, and carbon dioxide as products in alkaline media for a gold disk electrode [23]. A similar product distribution was also reported by Zhang et al. and Xi et al.[57] for the oxidation of glycerol on gold nanoparticles (2-6 nm) deposited on carbon and measured in the outlet of a Solid Anionic Membrane Fuel Cells.[58] In addition to the results presented by Zhang et al. and Xi et al.[57], recently few reports have also shown the influence of the support[59],

the particle size[60] and the loading[61] of the nanoparticles towards the glycerol oxidation. Unfortunately, the product distribution was not shown in any of these studies. Therefore a more extensive and detailed analysis of the nature of the reaction products generated with the shape controlled Au nanoparticles will be included in forthcoming contributions.

4. Conclusions

In this work, we have reported the synthesis of preferential oriented Au nanoparticles and their electrochemical activity towards the oxidation of small organic molecules in alkaline medium. The nanoparticles were characterized by X-ray diffraction, transmission electron microscopy and electrochemical methods. It was confirmed that the cubic nanoparticles present high ratio of (100) sites while octahedral particles present (111) preferential orientation.

The oxidation of a small organic molecule, such as carbon monoxide and methanol, did not present a clear surface structure sensitive effect. However, for the oxidation of formaldehyde, an evident surface structure effect is observed. In particular, at low potentials, the Au(111) nanoparticles presented higher activities, whilst the Au(100) nanoparticles were more active at higher potentials. In the case of the oxidation of larger molecules such as ethanol and glycerol, Au(111) nanoparticles clearly showed higher current densities, especially in the case of the glycerol oxidation, where currents were twice larger than those observed for the Au(100) ones.

5. Acknowledgement

P.R. acknowledges financial support from the Netherlands Organization for Scientific Research (NWO) through VENI grant and the University of Birmingham through the Birmingham Fellowship. The authors also acknowledge the Centre for Electron

Microscopy at the University of Birmingham for the support in the utilization of the microscopy facilities.

6. References

(1) Braunchweig, B.; Hibbitts, D.; Neurock, M.; Wieckowski, A. *Catalysis Today* **2013**, *202*, 197.

(2) Zhou, W. J.; Zhou, B.; Li, W. Z.; Zhou, Z. H.; Song, S. Q.; Sun, G. Q.; Xin, Q.; Douvartzides, S.; Goula, M.; Tsiakaras, P. *J. Power Sources* **2004**, *126*, 16.

(3) Lamy, C.; Lima, A.; LeRhun, V.; Delime, F.; Coutanceau, C.; Léger, J.-M. *J. Power Sources* **2002**, *105*, 283.

(4) Lamy, C.; Belgsir, E. M.; Leger, J. M. *Journal of Applied Electrochemistry* **2001**, *31*, 799.

(5) Santasalo-Aarnio, A.; Kwon, Y.; Ahlberg, E.; Kontturi, K.; Kallio, T.; Koper, M. T. M. *Electrochemistry Communications* **2011**, *13*, 466.

(6) Kwon, Y.; Schouten, K. J. P.; Koper, M. T. M. *Chemcatchem* **2011**, *3*, 1176.

(7) Kwon, Y.; Lai, S. C. S.; Rodriguez, P.; Koper, M. T. M. *J. Am. Chem. Soc.* **2011**, *133*, 6914.

(8) Lai, S. C. S.; Kleijn, S. E. F.; Ozturk, F. T. Z.; Vellinga, V. C. v. R.; Koning, J.; Rodriguez, P.; Koper, M. T. M. *Catalysis Today* **2010**, *154*, 92.

(9) Hernández, J.; Solla-Gullón, J.; Herrero, E.; Aldaz, A.; Feliu, J. M. *Electrochimica Acta* **2006**, *52*, 1662.

(10) Strmcnik, D.; Kodama, K.; van der Vliet, D.; Greeley, J.; Stamenkovic, V. R.; Markovic, N. M. *Nature Chemistry* **2009**, *1*, 466.

(11) Sitta, E.; Batista, B. C.; Varela, H. *Chemical Communications* **2011**, *47*, 3775.

(12) Casella, I. G.; Gatta, M.; Contursi, M. *Journal of Electroanalytical Chemistry* **2004**, *561*, 103.

(13) Macia, M. D.; Herrero, E.; Feliu, J. M.; Aldaz, A. *Journal of Electroanalytical Chemistry* **2001**, *500*, 498.

(14) Herrero, E.; Feliu, J. M.; Aldaz, A. *Journal of Electroanalytical Chemistry* **1994**, *368*, 101.

(15) Liu, Y.; Lowe, M. A.; DiSalvo, F. J.; Abruña, H. D. *The Journal of Physical Chemistry C* **2010**, *114*, 14929.

(16) Alden, L. R.; Han, D. K.; Matsumoto, F.; Abruña, H. D.; DiSalvo, F. J. *Chemistry of Materials* **2006**, *18*, 5591.

(17) Kang, Y.; Qi, L.; Li, M.; Diaz, R. E.; Su, D.; Adzic, R. R.; Stach, E.; Li, J.; Murray, C. B. *ACS Nano* **2012**, *6*, 2818.

(18) Lamy, C.; Rousseau, S.; Belgsir, E. M.; Coutanceau, C.; Leger, J. M. *Electrochimica Acta* **2004**, *49*, 3901.

(19) Jiang, L.; Colmenares, L.; Jusys, Z.; Sun, G. Q.; Behm, R. J. *Electrochimica Acta* **2007**, *53*, 377.

(20) Santiago, E. I.; Camara, G. A.; Ticianelli, E. A. *Electrochimica Acta* **2003**, *48*, 3527.

(21) Lebedeva, N. P.; Janssen, G. J. M. *Electrochimica Acta* **2005**, *51*, 29.

(22) Rodriguez, P.; Garcia-Araez, N.; Koverga, A.; Frank, S.; Koper, M. T. M. *Langmuir* **2010**, *26*, 12425.

(23) Gomes, J.; Tremiliosi-Filho, G. *Electrocatalysis* **2011**, *2*, 96.

(24) Rodriguez, P.; Koper, M. T. M. *Physical Chemistry Chemical Physics* **2014**, *16*, 13583.

(25) Simões, M.; Baranton, S.; Coutanceau, C. *ChemSusChem* **2012**, *5*, 2106.

(26) Zhang, Z.; Xin, L.; Li, W. *Applied Catalysis B: Environmental* **2012**, *119–120*, 40.

(27) Adžić, R. R.; Avramov-Ivić, M. *Journal of Catalysis* **1986**, *101*, 532.

(28) Avramov-Ivić, M. L.; Leger, J. M.; Lamy, C.; Jović, V. D.; Petrović, S. D. *Journal of Electroanalytical Chemistry and Interfacial Electrochemistry* **1991**, *308*, 309.

(29) Avramov-Ivic, M.; Adzic, R. R.; Bewick, A.; Razaq, M. *Journal of Electroanalytical Chemistry and Interfacial Electrochemistry* **1988**, *240*, 161.

(30) Rodríguez, P.; Koverga, A. A.; Koper, M. T. M. *Angewandte Chemie International Edition* **2010**, *49*, 1241.

(31) Rodriguez, P.; Garcia-Araez, N.; Koper, M. T. M. *Physical Chemistry Chemical Physics* **2010**, *12*, 9373.

(32) Rodriguez, P.; Feliu, J. M.; Koper, M. T. M. *Electrochemistry Communications* **2009**, *11*, 1105.

(33) Beyhan, S.; Uosaki, K.; Feliu, J. M.; Herrero, E. *Journal of Electroanalytical Chemistry* **2013**, *707*, 89.

(34) Hernandez, J.; Solla-Gullon, J.; Herrero, E.; Aldaz, A.; Feliu, J. M. *Electrochimica Acta* **2006**, *52*, 1662.

(35) Chen, Y.; Schuhmann, W.; Hassel, A. W. *Electrochemistry Communications* **2009**, *11*, 2036.

(36) Yahikozawa, K.; Nishimura, K.; Kumazawa, M.; Tateishi, N.; Takasu, Y.; Yasuda, K.; Matsuda, Y. *Electrochimica Acta* **1992**, *37*, 453.

(37) Yang, H.; Lu, T.; Xue, K.; Sun, S.; Lu, G.; Chen, S. *Journal of Molecular Catalysis A: Chemical* **1999**, *144*, 315.

(38) Sau, T. K.; Murphy, C. J. *J. Am. Chem. Soc.* **2004**, *126*, 8648.

(39) Kim, D.; Heo, J.; Kim, M.; Lee, Y. W.; Han, S. W. *Chemical Physics Letters* **2009**, *468*, 245.

(40) Heo, J.; Kim, D.-S.; Kim, Z. H.; Lee, Y. W.; Kim, D.; Kim, M.; Kwon, K.; Park, H. J.; Yun, W. S.; Han, S. W. *Chemical Communications* **2008**, 6120.

(41) Erikson, H.; Sarapuu, A.; Tammeveski, K.; Solla-Gullón, J.; Feliu, J. M. *ChemElectroChem* **2014**, *1*, 1338.

(42) Eguchi, M.; Mitsui, D.; Wu, H.-L.; Sato, R.; Teranishi, T. *Langmuir* **2012**, *28*, 9021.

(43) Hernández, J.; Solla-Gullón, J.; Herrero, E.; Feliu, J. M.; Aldaz, A. *Journal of Nanoscience and Nanotechnology* **2009**, *9*, 2256.

(44) Hernández, J.; Solla-Gullón, J.; Herrero, E. *Journal of Electroanalytical Chemistry* **2004**, *574*, 185.

(45) Hernández, J.; Solla-Gullón, J.; Herrero, E.; Aldaz, A.; Feliu, J. M. *The Journal of Physical Chemistry B* **2005**, *109*, 12651.

(46) Chen, Y.; Hassel, A.; Erbe, A. *Electrocatalysis* **2011**, *2*, 106.

(47) Hernandez Ferrer, J., Universidad de Alicante, 2008.

(48) Beden, B. L., J.M; Lamy, C. *Modern Aspects of Electrochemistry*; Springer Science & Business Media, 1992; Vol. 22.

(49) Angerstein-Kozlowska, H.; Conway, B. E.; Hamelin, A.; Stoicoviciu, L. *Journal of Electroanalytical Chemistry and Interfacial Electrochemistry* **1987**, *228*, 429.

(50) Borkowska, Z.; Tymosiak-Zielinska, A.; Shul, G. *Electrochimica Acta* **2004**, *49*, 1209.

(51) Assiongbon, K. A.; Roy, D. *Surface Science* **2005**, *594*, 99.

(52) Rodriguez, P.; Kwon, Y.; Koper, M. T. M. *Nat Chem* **2012**, *4*, 177.

(53) *F.J. Vidal-Iglesias et al (see reference below) have demonstrated that conventional TEM does not allow to discriminate between shape of the nanoparticles and the long order surface structure on the facets of the nanoparticles.* .

(54) Vidal-Iglesias, F. J.; Solla-Gullón, J.; Herrero, E.; Montiel, V.; Aldaz, A.; Feliu, J. M. *Electrochemistry Communications* **2011**, *13*, 502.

(55) Chang, S. C.; Hamelin, A.; Weaver, M. J. *The Journal of Physical Chemistry* **1991**, *95*, 5560.

(56) Edens, G. J.; Hamelin, A.; Weaver, M. J. *The Journal of Physical Chemistry* **1996**, *100*, 2322.

(57) Xin, L.; Zhang, Z.; Qi, J.; Chadderdon, D.; Li, W. *Applied Catalysis B: Environmental* **2012**, *125*, 85.
(58) Zhang, Z.; Xin, L.; Li, W. *International Journal of Hydrogen Energy* **2012**, *37*, 9393.
(59) Gomes, J. F.; Gasparotto, L. H. S.; Tremiliosi-Filho, G. *Physical Chemistry Chemical Physics* **2013**, *15*, 10339.
(60) Padayachee, D.; Golovko, V.; Ingham, B.; Marshall, A. T. *Electrochimica Acta* **2014**, *120*, 398.
(61) Marshall, A. T.; Golovko, V.; Padayachee, D. *Electrochimica Acta* **2015**, *153*, 370.

Figure Captions

Figure 1. X-Ray diffraction pattern of (A) Au cubic nanoparticles and (B) Au octahedral nanoparticles. The insets show the TEM images of the corresponding nanoparticles.

Figure 2. Voltammetric profiles of the cubic Au nanoparticles (dashed or dotted line) and octahedral Au nanoparticles (solid line) in (A) NaOH 0.1 M + $Pb(NO_3)_2$ 10^{-3} M and (B) NaOH 0.1 M . Scan rate υ= 50 mV s^{-1}.

Figure 3. Voltammetric profiles of the cubic Au nanoparticles (dashed or dotted line) and octahedral Au nanoparticles (solid line) in (A) 0.1 M NaOH + 2.5 M methanol and (B) 0.1 M NaOH + 0.1 formaldehyde. Scan rate υ= 50 mV s^{-1}.

Figure 4. Voltammetric profiles of the cubic Au nanoparticles (dashed or dotted line) and octahedral Au nanoparticles (solid line) in (A) 0.1 M NaOH +0.5 M ethanol and (B) 0.1 M NaOH + 0.01 M glycerol Scan rate υ= 50 mV s^{-1}.

Figures

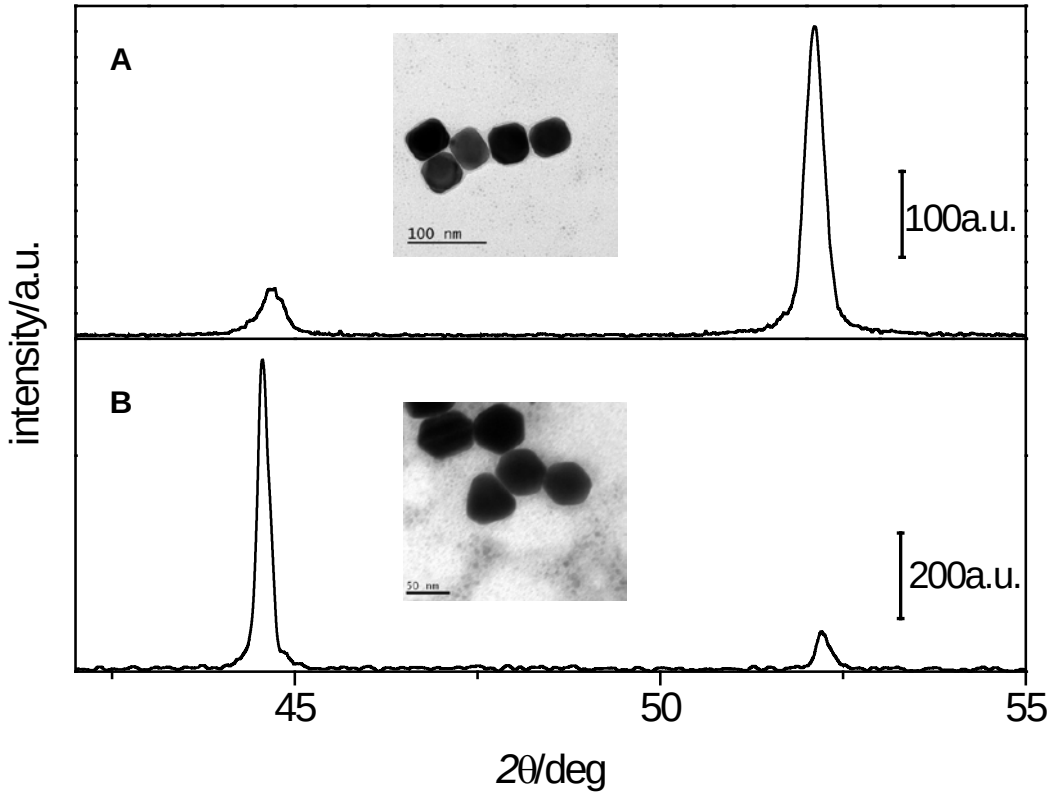

Figure 1.

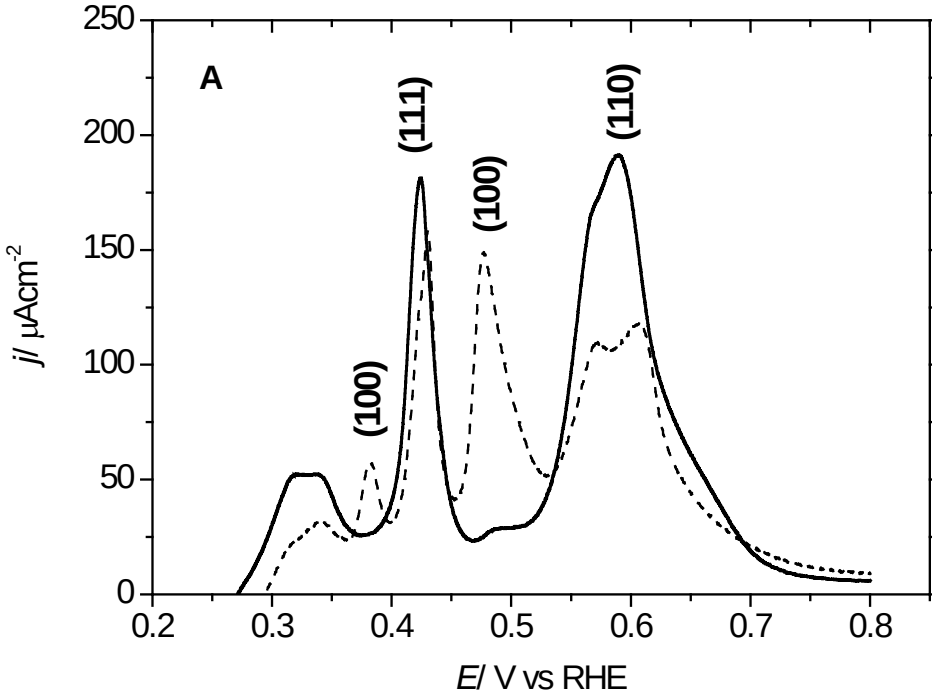
A
(100)
(111)
(100)
(110)
250
200
150
100
50
0
0.2
0.3
0.4
0.5
0.6
0.7
0.8
j/ µAcm-2
E/ V vs RHE

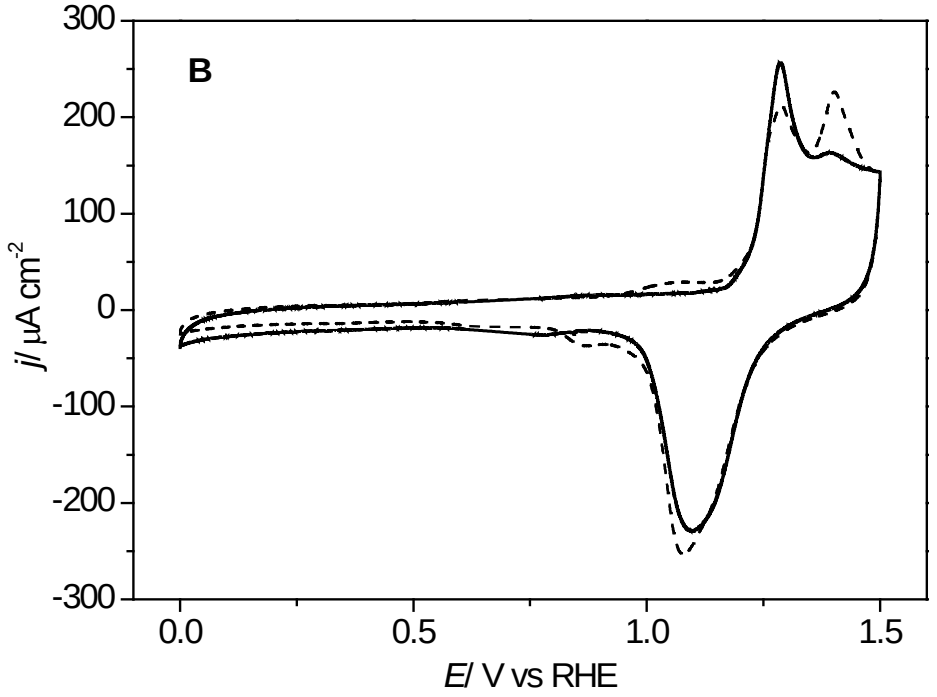
B
300
200
100
0
-100
-200
-300
0.0
0.5
1.0
1.5
j/ µA cm-2
E/ V vs RHE

Figure 2.

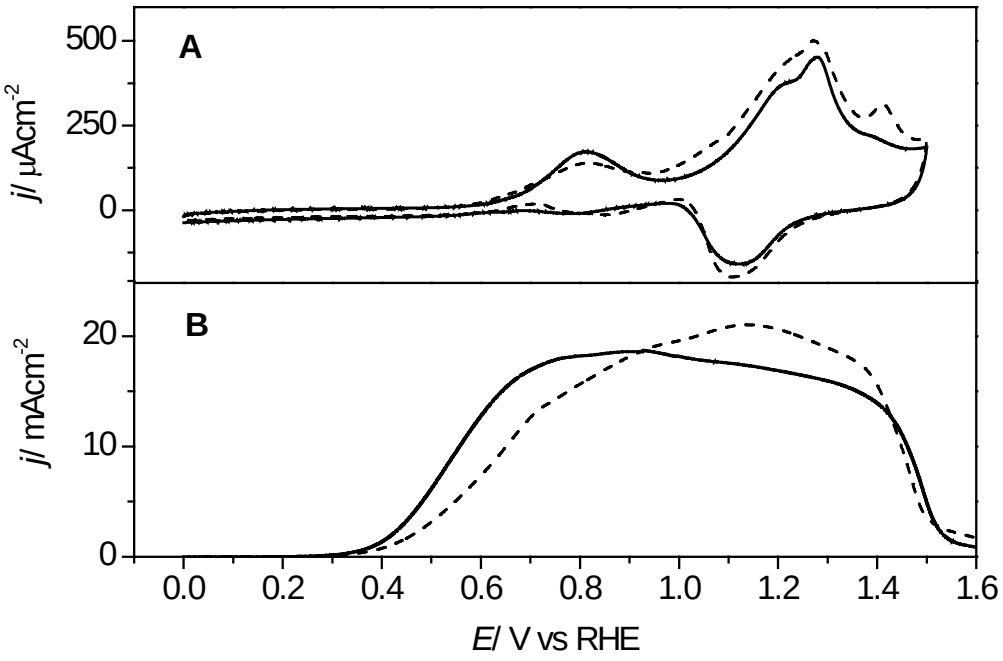
A
B
500
250
0
20
10
0
0.0
0.2
0.4
0.6
0.8
1.0
1.2
1.4
1.6
j/ µAcm-2
j/ mAcm-2
E/ V vs RHE

Figure 3.

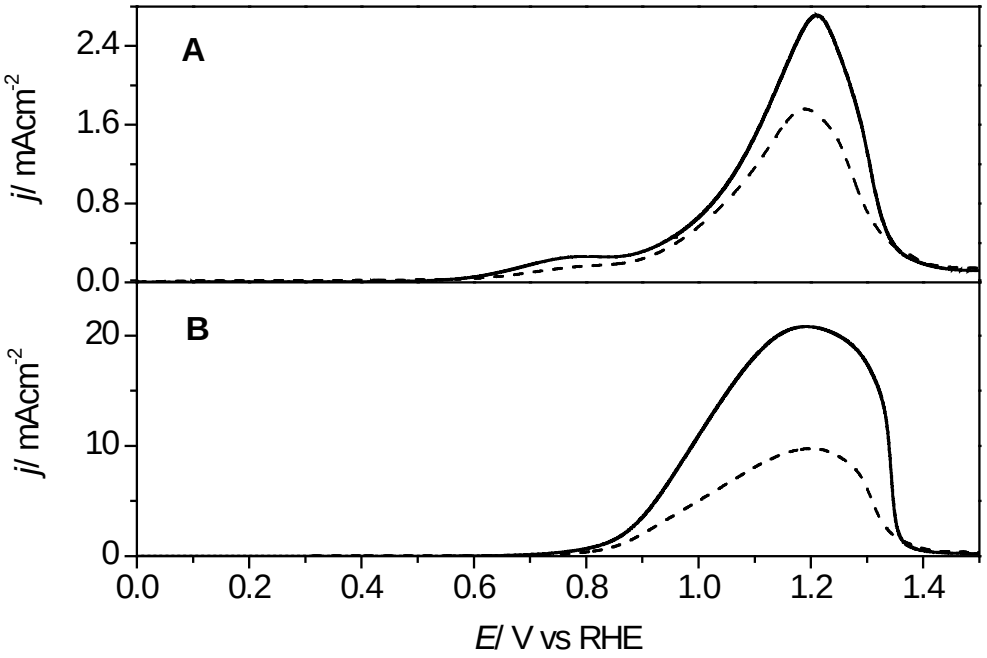
A
B
2.4
1.6
0.8
0.0
20
10
0
j/ mAcm-2
j/ mAcm-2
0.0
0.2
0.4
0.6
0.8
1.0
1.2
1.4
E/ V vs RHE

Figure 4.